A New Interleukin-13 Amino-Coated Gadolinium Metallofullerene Nanoparticle for Targeted MRI Detection of Glioblastoma Tumor Cells

Tinghui Li,[†,‡,⊥] Susan Murphy,[†,⊥] Boris Kiselev,[†,‖] Kanwarpal S. Bakshi,[†,‖] Jianyuan Zhang,[†,‡] Amnah Eltahir,[†,‡] Yafen Zhang,[‡] Ying Chen,[‡] Jie Zhu,[‡] Richey M. Davis,[§] Louis A. Madsen,[‡] John R. Morris,[‡] Daniel R. Karolyi,[†,‖] Stephen M. LaConte,[†] Zhi Sheng,*[,†] and Harry C. Dorn*[,†,‡]

[†]Virginia Tech Carilion Research Institute, Roanoke, Virginia 24016, United States

[‡]Department of Chemistry, and [§]Department of Chemical Engineering, Virginia Polytechnic Institute and State University, Blacksburg, Virginia 24061, United States

[‖]Virginia Tech Carilion School of Medicine, Roanoke, Virginia 24016, United States

S *Supporting Information*

ABSTRACT: The development of new nanoparticles as next-generation diagnostic and therapeutic ("theranostic") drug platforms is an active area of both chemistry and cancer research. Although numerous gadolinium (Gd) containing metallofullerenes as diagnostic magnetic resonance imaging (MRI) contrast agents have been reported, the metallofullerene cage surface, in most cases, consists of negatively charged carboxyl or hydroxyl groups that limit attractive forces with the cellular surface. It has been reported that nanoparticles with a positive charge will bind more efficiently to negatively charged phospholipid bilayer cellular surfaces, and will more readily undergo endocytosis. In this paper, we report the preparation of a new functionalized trimetallic nitride template endohedral metallofullerene (TNT EMF), $Gd_3N@C_{80}(OH)_x(NH_2)_y$, with a cage surface bearing positively charged amino groups ($-NH_3^+$) and directly compare it with a similar carboxyl and hydroxyl functionalized derivative. This new nanoparticle was characterized by X-ray photoelectron spectroscopy (XPS), dynamic light scattering (DLS), and infrared spectroscopy. It exhibits excellent ^1H MR relaxivity. Previous studies have clearly demonstrated that the cytokine interleukin-13 (IL-13) effectively targets glioblastoma multiforme (GBM) cells, which are known to overexpress IL-13Rα2. We also report that this amino-coated Gd-nanoplatform, when subsequently conjugated with interleukin-13 peptide IL-13-$Gd_3N@C_{80}(OH)_x(NH_2)_y$, exhibits enhanced targeting of U-251 GBM cell lines and can be effectively delivered intravenously in an orthotopic GBM mouse model.
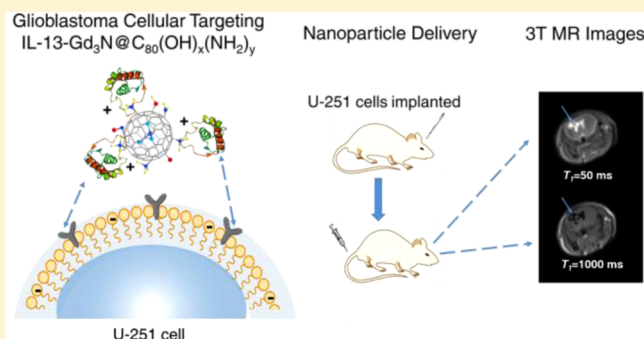
1. INTRODUCTION

Cancer is one of the most destructive diseases known to mankind, and glioblastoma multiforme (GBM) is no exception. GBM is a stage 4/4 astrocytoma, and it is the most common primary brain tumor in adults. GBM has the worst prognosis of any central nervous system (CNS) malignancy; the median survival rate is approximately one year, and less than 5% of patients diagnosed with GBM live longer than 5 years.[1] Throughout the past few years, efforts have been made in order to develop methods that specifically target cancerous cells. Specifically, nanoparticle mediated delivery of drug and diagnostic contrast material has shown tremendous potential for crossing physiologic barriers,[2] enhancing bioavailability, and enabling precise targeting.[3,4] Endohedral metallofullerenes (EMFs) represent a unique class of nanoparticles that are highly stable and resistant to opening by most biological

processes.[5−10] EMFs are also advantageous as the spheroidal carbon cage structure leads to a high surface-to-volume ratio. This allows for multiple functional groups to be attached to the surface of the sphere, enhancing the potential for nanoparticles with targeting, diagnostic, and therapeutic modalities.

It has been previously established that neutral and negatively charged nanoparticles are generally less effective in crossing cell membranes than positively charged nanoparticles.[1,11−13] Numerous gadolinium-containing EMFs as diagnostic magnetic resonance imaging (MRI) contrast agents have been reported and are very promising materials that confine the toxic Gd^{3+} ions inside an inert, robust, carbon cage. These nanoplatforms exhibit 10−40 times higher ^1H relaxivity than most commercial

contrast agents.[14] Seminal studies by Shinohara and co-workers[14,15] and Wilson and co-workers[16,17] focused on monometal EMFs, namely, $Gd@C_{82}$ and $Gd@C_{60}$, with the metallofullerene cage surfaces consisting of negatively charged carboxyl or hydroxyl groups. In the past few years, considerable attention has focused on the trimetallic nitride template endohedral metallofullerenes (TNT EMFs)[6,18−20] and many water-soluble derivatives of $Gd_3N@I_h$-C_{80}. Gd-containing mixed metal TNT EMFs have been synthesized and recently reviewed as MRI contrast agents.[5−8,20−22] Earlier studies by Debinski and collaborators have shown that the cytokine interleukin-13 (IL-13), together with its receptor, is overexpressed in human GBM cell lines and GBM tissue but not in normal brain tissue.[23,24] We have previously reported a TNT EMF platform of $Gd_3N@C_{80}$ functionalized with carboxyl groups, and conjugated to interleukin-13, IL-13-$Gd_3N@$ $C_{80}(OH)_{26}(CH_2CH_2COOM)_{16}$ ((IL-13-carboxyl)-**IIa**). Unfortunately, this nanoparticle was intracranially delivered to GBM xenograft mice models (U-87) via invasive convection enhanced delivery (CED).[25] In most cases reported to date, the metallofullerene nanoparticle cage surface consists of negatively charged carboxyl or hydroxyl groups that limit attractive forces on the cellular surface (Figure 1). A notable exception is
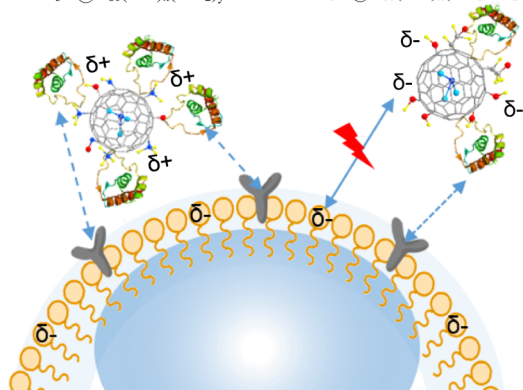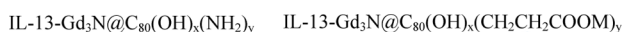

Figure 1. IL-13-$Gd_3N@C_{80}(OH)_x(NH_2)_y$ nanoparticle with positive charges illustrating facile binding to a negatively charged phospholipid bilayer cellular surfaces.

demonstrated by Zheng and co-workers[26] reporting the preparation of the MRI contrast agent $Gd@$ $C_{82}O_{14}(OH)_{14}(NH_2)_6$, where, under physiological conditions, the cage surface is expected to exhibit a positive charge due to the presence of $(-NH_3)^+$ groups.

In this paper, we report a new functionalization procedure for the $Gd_3N@C_{80}$ platform providing trimetallic nitride $Gd_3N@C_{80}(OH)_x(NH_2)_y$ ((amino)-**I**). This was characterized by X-ray photoelectron spectroscopy (XPS), dynamic light scattering (DLS), and infrared spectroscopy, and exhibits excellent ^{1}H MR relaxivity. This new Gd-nanoplatform, when conjugated with an interleukin-13 peptide, shows enhanced targeting of U-251 GBM cell lines. In addition, we demonstrate that the $Gd_3N@C_{80}$ platform can be successfully conjugated to an IL-13-TAMRA peptide that displays effective targeting of orthotopic GBM xenografts in mice by intravenous delivery. Our hypothesis is that the (amino)-**I** positively charged nanoparticle and IL-13 targeting peptide exhibit enhanced charge attraction for GBM cellular endocytosis, due to multireceptor site binding and the presence of positively

charged amino groups $(-NH_3^+)$ on the metallofullerene cage surface (Figure 1). In addition, we show enhanced noninvasive intravenous delivery and MRI targeting of $Gd_3N@$ $C_{80}(OH)_x(NH_2)_y$ ((amino)-**I**) to U-251 tumors implanted in a mouse model.

2. EXPERIMENTAL PROCEDURES

Preparation of Functionalized $Gd_3N@C_{80}$ ((Amino)-I). The functionalization of the amino group onto $Gd_3N@C_{80}$, (amino)-**I**, was performed following a recently reported procedure.[26] Briefly, $Gd_3N@$ C_{80} (ca. 5 mg) was added to 246 μL of 50 wt % H_2O_2 and 180 μL of 28 wt % NH_4OH. The mixtures were vigorously stirred at 50 °C under ambient conditions for 1.5 h. At the end of the reaction, the black suspension turned to a yellow solution. The yellow solution was mixed with ethanol to remove the excess H_2O_2 and NH_4OH, and the amount ratio between supernatant and ethanol was 1:12. The suspension was centrifuged at 10 000 rpm for 10 min, and the yellowish precipitate was collected and washed with an excess amount of ethanol and then dried under vacuum at 50 °C for 24 h.

Conjugation of IL-13-TAMRA-$Gd_3N@$ $C_{80}O_{12}(OH)_{10}(NH_2)_7(NO_2)_2$ ((IL-13-Amino)-Ia). The TAMRA-VDKLLLHLKKLFREGQFNREGQFNRNFESIIICRDRT-OH, a shorter active peptide for IL-13Rα2 receptor sites, instead of the complete IL-13 sequence was obtained from New England Peptide LLC, Gardner, MA, (Figure S1).[25] This shorter peptide was dissolved in dimethyl sulfoxide (DMSO) at a concentration of 2 mg/mL. Dissolving the peptide in DMSO instead of water represented a significant change from previous work,[22,25] and led to greater solubility of the peptide. For the conjugation reaction, (amino)-**I** was diluted in 2-(N-morpholino)ethanesulfonic acid (MES), and filtered through a 0.45 μm syringe filter. The carboxyl groups of the IL-13-TAMRA were activated by 66 μL of 2 mM 1-ethyl-3-[3-(dimethylamino)propyl] carbodiimide hydrochloride (EDC) and the same amount of N-hydroxysulfosuccinimide (Sulfo-NHS). After 10 min, 500 μL of functionalized $Gd_3N@C_{80}$ was added and incubated at room temperature for 1.5 h. Subsequently, 66 μL of 0.275 mM hydroxyl amine was added to quench the reaction (Figure 2). The resulting
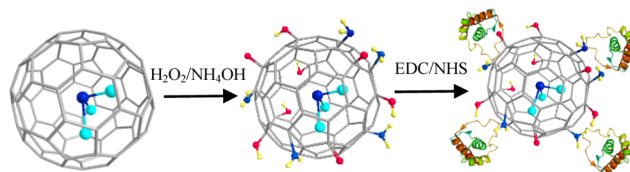

Figure 2. Functionalization and conjugation process of $Gd_3N@C_{80}$. The hydrophobic $Gd_3N@C_{80}$ reacts with H_2O_2 and NH_4OH, providing aqueous colloidal stability (amino)-**I**. The second step conjugates the functionalized gadofullerene molecule to the IL-13 peptide with fluorescent tagging through amide bond formation (IL-13-amino)-**Ia** (gray, carbon; aqua, gadolinium ion; blue, nitrogen; red, oxygen; yellow, hydrogen).

solution was filtered through Zeba-brand spin columns at a rate of 5000 rpm for 2 min. The receptacle portion of the spin column was thoroughly rinsed with solution to ensure that all the (IL-13-amino)-**Ia** product was removed from the column. Based on inductively coupled plasma mass spectroscopy (ICP-MS), the Gd^{3+} concentration of (IL-13-amino)-**Ia** was 1.98 μM.

IL-13-TAMRA-$Gd_3N@C_{80}(OH)_{26}(CH_2CH_2COOM)_{16}$ (IL-13-Carboxyl)-IIa). A volume of 500 μL of (carboxyl)-**II** was dissolved in MES solution, and a concentration of approximately 50 μM was filtered through a 0.45 μm syringe filter. The carboxyl groups were activated via addition of 70 μL of 0.5 M EDC and 70 μL of 0.5 M Sulfo-NHS to the f-$Gd_3N@C_{80}$ solution. After 10 min, 85 μL of the IL-13-TAMRA peptide (dissolved in DMSO) was added, and the reaction was continued for 1.5 h. After this time, 70 μL of hydroxyl-amine solution was added to quench the reaction. The resulting
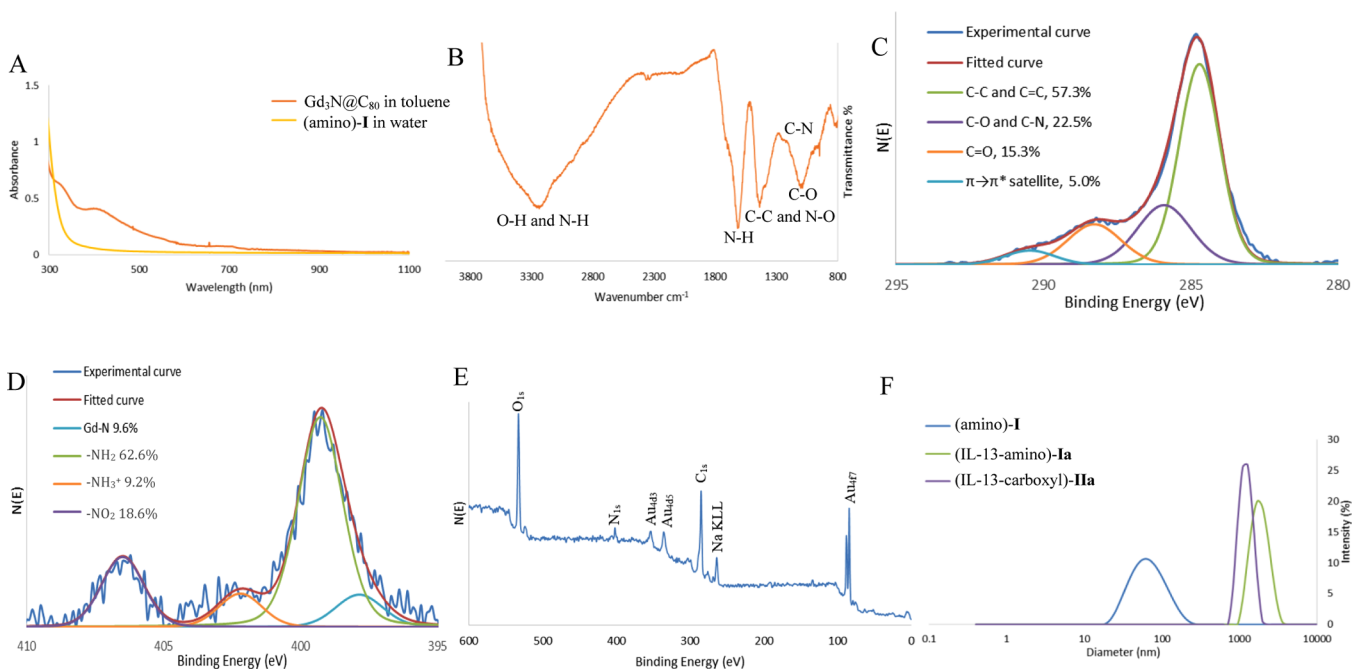
Figure 3. Characterization of the functionalized $Gd_3N@C_{80}$. (A) Electronic absorption spectra of $Gd_3N@C_{80}$ before and after functionalization. (B) RAIRS spectrum of (amino)-**I**. (C, D) XPS multiplex spectra of the (amino)-**I**. (E) The XPS survey spectrum of (amino)-**I**. Au was used for calibration. (F) Hydrodynamic size distribution of (amino)-**I**, (IL-13-amino)-**Ia**, and (IL-13-carboxyl)-**IIa** in water.

solution was filtered through Zeba-brand spin columns at a rate of 5000 rpm for 2 min. The receptacle portion of the spin column was thoroughly rinsed to ensure that all the product was removed from the column. Based on ICP-MS, the Gd^{3+} concentration of (IL-13-carboxyl)-**IIa** was 0.47 μM.

Preparation of Scrambled ILs-13-TAMRA-Gd₃N@C₈₀O₁₂(OH)₁₀(NH₂)₇(NO₂)₂ (ILs-13-Amino)-Is) and ILs-13-TAMRA-Gd₃N@C₈₀(OH)₂₆(CH₂CH₂COOH)₁₆ (ILs-13-Carboxyl)-IIs). Both the amino functionalized nanoparticle and the carboxyl functionalized nanoparticle were conjugated with a scrambled IL-13 peptide, provided by American Peptide Company, Inc., Sunnyvale, CA. The same conjugation procedure described above was used to prepare the nanoparticles, (ILs-13-amino)-**Is** and (ILs-13-carboxyl)-**IIs**.

Characterization of Functionalized Gd₃N@C₈₀ and IL-13-TAMRA-Functionalized Gd₃N@C₈₀. The (amino)-**I** was further characterized by XPS, DLS, and infrared spectroscopy. The (IL-13-amino)-**Ia** sample was characterized by DLS and confocal microscopy.

Relaxivity Measurements for Functionalized Gd₃N@C₈₀. The T_1 and T_2 relaxation times were measured on Bruker Minispec mq 20 (0.47 T), mq 60 (1.41 T) analyzers and a Bruker Avance III 400 MHz (9.4 T) wide bore spectrometer equipped with an MIC 400 W1/S2 probe and 5 mm ^{1}H coil. The inversion−recovery method was used to measure the spin−lattice relaxation time T_1, and the Carr−Pucell−Meiboom−Gill method was used for the spin−spin relaxation time T_2 measurement. Errors in T_1 and T_2 values were less than ±2%. Solutions with different Gd^{3+} concentrations were prepared by diluting a stock solution with deionized water. The concentration of the Gd^{3+} ions was determined by ICP-MS.

Confocal Microscopy Comparison Study of Nanoparticles with U-251 Cell Lines (Increased IL-13Rα2 Expression) and with HeLa Cell Lines (No Overexpression of IL-13Rα2). Cells (U-251 or HeLa 5×10^4 cells/well) were inoculated in four-well chamber slides and incubated overnight. The (IL-13-amino)-**Ia**, (IL-13-carboxyl)-**IIa**, scrambled (ILs-13-amino)-**Is**, and scrambled (ILs-13-carboxyl)-**IIs** nanoparticles (0.75 μM/well) were added to each well, incubated 20 min at 37 °C, washed, stained with Hoechst (1:15 000, 37 °C, 10 min), washed again, and fixed with 4% buffered paraformaldehyde (37 °C, 30 min).

High-magnification optical sections were captured with a Leica spinning disk laser confocal microscope (LCM) equipped with a 63× oil-immersion objective. The microscope model, objective, pinhole, gain, and black level settings were held constant for each experiment. Fluorescence from Hoechst and TAMRA was generated by exciting the samples with laser lines from a blue diode (405 nm) and green HeNe (543 nm) lasers. The fluorescence emission was collected simultaneously in two separate photomultipliers with the spectrophotometer scan head detector windows set to ranges of 413−502 nm (for Hoechst) and 562−700 nm (for TAMRA). The acousto-optic tunable filter was adjusted to ensure that there was no crosstalk of signal between channels when fluorescence was collected from each channel simultaneously.

For quantitative analyses of TAMRA internalization and cellular distribution, confocal optical sections (z-stacks) were taken in at least four fields per slide, 1−2 μm thickness.

Introduction of Glioblastoma Cells to Nude Athymic Mouse Model. In vivo orthotopic xenograft U-251 cell implantation experiments involving the use of mice were carried out in accordance with protocols approved by the Virginia Tech Institutional Animal Care and Use Committee. Female SCID/beige 7−8 week old mice were anesthetized with isoflurane (2−4%) and placed in a stereotactic frame (World Precision Instruments). The incision site at the top of the head was disinfected with betadine and alcohol. After a midline incision, a burr hole was made in the skull 0.5 mm anterior to the bregma and 2 mm laterally to the appropiate hemisphere. A 25 μL Hamilton syringe was used to inject 2×10^5 GBM cells (U-251), suspended in 4 μL PBS, 4 mm deep from the surface of the skull. The injection was made over 5 min using a microinfusion pump. The needle was left in place for another 3 min before withdrawing. The burr hole was sealed with bone wax, and the incision closed using size 4 sutures.

After the procedure animals were weighed daily and monitored carefully for signs of increased intracranial pressure from the growing tumor mass. Thirty days after the introduction of the tumor cells, the IL-13-TAMRA-functionalized-$Gd_3N@C_{80}$ nanoparticle was administered to the animals using either a convection enhanced delivery (CED) approach or an intravenous approach.

Administration of IL-13-TAMRA-Functionalized Gd₃N@C₈₀ to Xenografted Mice. The CED method of administration of (IL-13-carboxyl)-**IIa** nanoparticles has been reported by Fillmore and co-workers.[25] To perform this procedure, one group of animals were

anesthetized via isoflurane and placed in the stereotactic frame. The burr hole from the injection of the tumors was identified, and a Hamilton syringe was inserted through it to a depth of 4 mm from the surface of the skull. A volume of 18 μL of (IL-13-carboxyl)-**IIa** nanoparticle was injected at a rate of 0.2 μL/min (total injection time of 90 min). During administration of the agent, the animal was maintained under anesthesia via isoflurane 1−3% and was carefully monitored. After the full dose of agent was administered the syringe was carefully removed and the incision closed. The animal was given buprenorphine for pain control and monitored for recovery, and then returned to the vivarium.

A second group of animals received either (IL-13-amino)-**Ia** or (IL-13-carboxyl)-**IIa** nanoparticles via an intravenous tail vein delivery method. This method of administering the functionalized EMFs for the purpose of brain tumor targeting has not been previously reported and represents a major shift from the invasive intracranial CED delivery of the nanoparticles previously reported (vide supra). A volume of 250 μL of (IL-13-carboxyl)-**IIa** was injected into the tail vein of the mouse using a tail vein illuminator (Braintree Scientific). One mouse was administered (IL-13-amino)-**Ia** (3 μM in 300 μL) via the tail vein. A volume of 300 μL of 500 μM Magnevist was intravenously delivered into another mouse. Approximately, 15 min after the mice were sacrificed, MRI images were obtained in a clinical 3 T MRI scanner.

In Vitro and in Vivo MRI Study of the Functionalized Gd$_3$N@ C$_{80}$, IL-13-Amino-Ia, and IL-13-carboxyl-IIa. The in vitro inversion−recovery MR images were obtained for the visual confirmation of the efficiency of the (amino)-**I** working as a contrast agent. A 3 T (123 MHz) clinical scanner was used. Various concentrations of the (IL-13-amino)-**Ia**, (IL-13-carboxyl)-**IIa**, (amino)-**I**, and the Magnevist were used and compared. To demonstrate clinical MRI feasibility, U-251 GBM cells orthotopically implanted in mice with (IL-13-amino)-**Ia**, (IL-13-carboxyl)-**IIa**, or Magnevist were also examined with a clinical 3 T MRI Siemens scanner, utilizing a wrist hand receiver coil.

3. RESULTS AND DISCUSSION

As previously indicated, transport, targeting, and cellular uptake are key considerations in the design of new "theranostic" nanoparticles for clinical cancer applications. In the present study, we have synthesized (as outlined in Figure 2) a new amino-functionalized nanoparticle, (amino)-**I**, which is significantly different from previously reported hydroxyl and carboxyl TNT EMF derivatives, (carboxyl)-**II**.[5] The electronic absorption spectrum for (amino)-**I** clearly exhibits the loss of π conjugation in comparison with the precursor EMF, Gd$_3$N@ C$_{80}$, as illustrated in Figure 3A. In the reflection absorption infrared spectroscopy (RAIRS) spectrum (Figure 3B) for (amino)-**I**, the characteristic vibration bands of broad overlapping O−H and N−H centered at (3236 cm^{-1}), N−H (1613 cm^{-1}), C−N (1224 cm^{-1}), and C−O (1086 cm^{-1}) suggest the existence of both hydroxyl and amino groups on the carbon cage. The strong peak centered at 1436 cm^{-1} suggests overlap of the C−C stretching vibration and N−O stretching vibration, which indicates the presence of nitro groups introduced onto the carbon cage. The XPS multiplex spectra for (amino)-**I** are presented in Figure 3C and D for the C$_{1s}$ and N$_{1s}$ regions, respectively. The C$_{1s}$ peaks, centered at binding energy values of 284.5, 286.4, and 290.6 eV, were assigned to the C−C, C−O (C−N), and $\pi \rightarrow \pi^*$ satellite, respectively. Since there is an obvious absence of a carbonyl absorption band in the RAIRS spectrum, the peak located at the binding energy of 288.1 eV is likely due to hemiketal or hemiacetals (RO-C−OH), or cyclic ether (C−O−C) structures.[27,28] The N$_{1s}$ peaks centered at 399.3 and 402.2 eV correspond to the free amino group (−NH$_2$) and partially protonated amino group (−NH$_3^+$),

indicating that amino groups have been successfully introduced to the carbon cages. Finally, the peak at the binding energy of 397.9 eV can be assigned to the metal nitride (Gd−N) group encapsulated in the carbon cage. It is worth noting that a new peak appears at around 406.5 eV that is assigned to the nitro group, which is significantly different from the previously reported Gd@C$_{82}$ case.[29,30] Based on the resulting atomic percentage of carbon and nitrogen (Tables S1 and S2), and the peak deconvolution of the XPS profile, the average formula for (amino)-**I** can be described as Gd$_3$N@ C$_{80}$O$_{12}$(OH)$_{10}$(NH$_2$)$_7$(NO$_2$)$_2$. Figure 3E shows the survey XPS spectrum of (amino)-**I**. The peaks centered at 285, 402, and 533 eV reveal the presence of C, N, and O species in the compound. The residue of Na KLL peak was from water.

It is well established that water-soluble metallofullerene derivatives form aggregates in water.[31] The DLS results for (amino)-**I** (Figure 3F) indicate that the hydrodynamic size of an aggregate nanoparticle is ∼60 nm in pure water. This is similar to the results previously reported for carboxylated and hydroxlated nanoparticles,[5] including polyethylene glycol− (PEG) functionalized derivatives as well as hydroxylated, Gd$_3$N@C$_{80}$.[8,9] As expected, after conjugation, the (IL-13-amino)-**Ia** exhibits a significant increase to ∼1880 nm in water, somewhat larger than the (IL-13-carboxyl)-**IIa** nanoparticle (∼1400 nm). The zeta potential provides a convenient approach to assess the surface charge on nanoparticles. Kardys and co-workers recently reported an amino-functionalized silica nanoparticle (SiNPs) that exhibited preferential uptake in pancreatic cancer cells.[12] In their study, the synthetic inclusion of positively charged −NH$_2$ groups increased the zeta potential from −45 to −31 mV. In similar fashion, our results also exhibit an increase in the zeta potential for the amino group nanoparticle (IL-13-amino)-**Ia** (6.46 mV) in comparison with the (IL-13-carboxyl)-**IIa** nanoparticle (−3.43 mV). It should also be noted that the unconjugated nanoparticle, (amino)-**Ia**, exhibits a zeta potential of −31.0 mV, which is close to the Kardys value (vide supra) and also a similar amino Gd$_3$N@C$_{80}$ metallofullerene nanoparticle reported by Kepley and co-workers.[32]

In previous studies, we have reported that the (IL-13-carboxyl)-**IIa** nanoparticle targets the GBM U-87 cell line.[22,25] In the current study, we employed the U-251 cell line which have the highest expression of IL-13Rα2 receptor sites of all GBM cell lines and are histologically similar to human GBM.[33,34] In order to ensure specific targeting of the U-251 cell line, we treated HeLa cells which do not overexpress the IL-13Rα2 receptor sites. The HeLa and U-251 cells were incubated with the same concentration of (IL-13-amino)-**Ia** and (IL-13-carboxyl)-**IIa**, respectively. As illustrated in Figure 4 and Supporting Information Figure S2, no colocalization of TAMRA with the HeLa cells was observed.

For the U-251 cells treatment, the nanoparticles are internalized by the U-251 cell line and a clear preference for localization in the nucleus is illustrated for both the (IL-13-amino)-**Ia** and (IL-13-carboxyl)-**IIa**, with a greater intensity in the former case (Figure 5). In a direct fluorescence quantitation (two-way ANOVA, Graphpad), there is a slight preponderance of (IL-13-amino)-**Ia** in the cytoplasm and cell membrane that is significantly enhanced in the nucleus in comparison with cells treated with (IL-13-carboxyl)-**IIa** (Figure 6). Thus, the nanoparticles coated in amino groups have high cell membrane binding affinity, readily translocate across the plasma membrane, and undergo endocytosis. This translocation
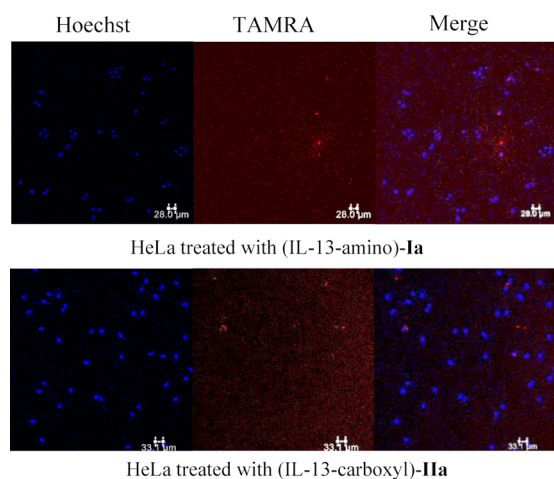
Figure 4. Images are projections of confocal *z*-stacks generated from sections of 5−6 *μ*m thickness comparing internalization of TAMRA in HeLa cells. Top row is HeLa treated with (IL-13-amino)-**Ia**, and bottom row is HeLa treated with (IL-13-carboxyl)-**IIa**.
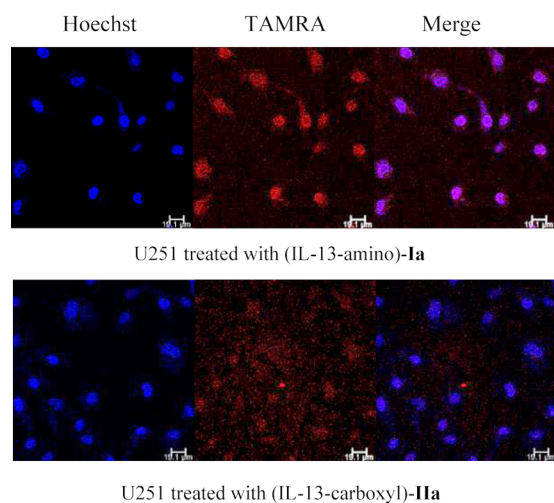

Figure 5. Images are projections of confocal *z*-stacks, generated from sections of 5−6 *μ*m thickness, comparing internalization of TAMRA in U-251 cells. 63× images z5; 10 images were taken 5 *μ*m apart. Scale bar = 19.1 *μ*m. Top row is U-251 treated with (IL-13-amino)-**Ia**, and bottom row is U-251 treated with (IL-13-carboxyl)-**IIa**.

process is illustrated in Figure 6 and explains why after a significant time interval (20−30 min) the fluorescence of (IL-13-amino)-**Ia** and (IL-13-carboxyl)-**IIa** is significantly concentrated in the nucleus in comparison with the cytoplasm and cell membrane.

   In order to demonstrate that the cell targeting specificity is due to the IL-13 peptide and not the f-Gd$_3$N@C$_{80}$ platform, the U-251 cells were also treated with a scrambled peptide analogue, (ILs-13-amino)-**Is** and (ILs-13-carboxyl)-**IIs**. Figure S3 shows that the scrambled peptide analogue (ILs-13-f-Gd$_3$N@C$_{80}$)-**Is** is not internalized by the U-251 cell line; therefore, the specific IL-13 peptide is necessary to specifically bind to cells that express the interleukin receptor site, IL-13Rα2. These results support our hypothesis that although both nanoparticles (**Ia** and **IIa**) display targeting to the U-251 cell line, the (IL-13-amino)-**Ia** positively charged nanoparticle exhibits enhanced targeting for GBM cells in comparison with the (IL-13-carboxyl)-**IIa** (Figures 1 and 6).
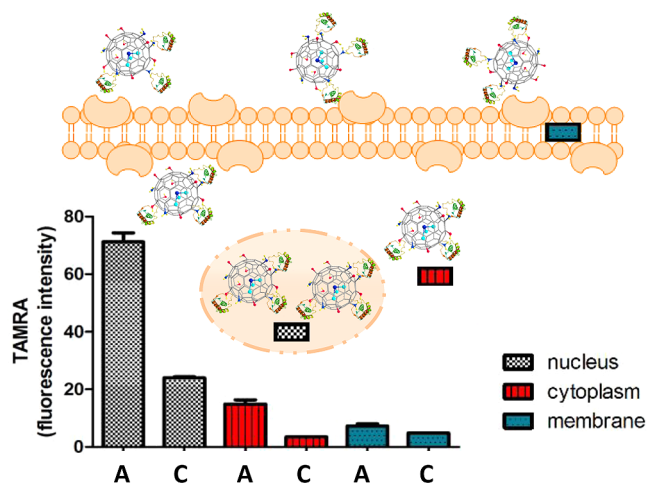

Figure 6. Translocation of (IL-13-amino)-**Ia** (A) and (IL-13-carboxyl)-**IIa** (C) in U-251 cells. Quantitation of TAMRA fluorescence by two-way ANOVA (GraphPad).

   Although the confocal microscopic studies (vide supra) illustrate effective targeting of U-251 GBM cell lines by both the (IL-13-amino)-**Ia** and (IL-13-carboxyl)-**IIa** nanoparticles, demonstration of effective transport of a targeting nanoparticle across the blood-brain barrier (BBB) by noninvasive intravenous delivery is critically important in the development of a new clinical GBM MRI contrast agent. Thus, GBM U-251 cells were orthotopically implanted in mice and, 30 days following the implantation of the xenograft tumor, the (IL-13-carboxyl)-**IIa** nanoparticle was administered to the mice using two approaches. In one approach, the nanoparticle agent (**IIa**) was administered intracranially to the implanted tumor site by CED, as described in earlier studies.[25] In a second approach, the nanoparticle (**IIa**) was delivered by systemic intravenous delivery via the tail vein. In a very limited biodistribution study for only the (IL-13-carboxyl)-**IIa** nanoparticle, we have measured the gadolinium concentration (ICP-MS) found for these nanoparticles after intravenous delivery in other organs besides the brain including the liver, spleen, and kidney. However, an important feature of this limited data is the significantly higher concentration of nanoparticles in the brain hemisphere containing the implanted tumor in comparison with the contralateral brain hemisphere. This is confirmed by the confocal microscopy and MRI as illustrated below. There is significant evidence of the (IL-13-carboxyl)-**IIa** nanoparticle at the implanted tumor site by confocal microscopy of tissue slices after the animals were sacrificed. For the (IL-13-carboxyl)-**IIa** nanoparticle (Figure S4), the TAMRA label is specifically observed at the brain tumor (T) site. For the case of systemic delivery (Figure S5), the nanoparticle can be observed at the edge of the tumor, but not in the necrotic center of the tumor. There is also evidence of increased fluorescence at distances removed from the primary tumor site suggesting detection of micrometastatic tumors. A more comprehensive study will be necessary to quantify the biodistribution of these targeting nanoparticles. These results complement the compelling (IL-13-amino)-**Ia** MRI results (vide infra) and provide evidence that both of these nanoparticles can be delivered by the less invasive intravenous tail vein injection with specific targeting to GBM U-251 mice brain tumor models.

   The ^{1}H MR r_1 relaxivity results for (amino)-**I** and (carboxyl)-**II** are summarized in Table 1, and the r_2 relaxivity results are

Table 1. Comparison of r_1 Relativities of Gadolinium Metallofullerenes (Units of mM^{-1} s^{-1} per mM in Pure Water at 298 K)

compd	r_1 relaxivity (mM^{-1} s^{-1})			hydrodynamic size (nm)
	0.35−0.5 T	1.0−3.0 T	7.1−9.4 T	
Gd$_3$N@C$_{80}$O$_{12}$(OH)$_{10}$(NH$_2$)$_7$(NO$_2$)$_2$ (amino)-**I**	88 ± 1 (0.47 T)	101. ± 0.5 (1.4 T)	30.5 (9.4 T)	60
Gd@C$_{82}$O$_{14}$(OH)$_{14}$(NH$_2$)$_6$[a][26]	47.0 (0.5 T)	41.0 (1.5 T), 39.5 (3 T)	27.4 (7.1 T)	16
Gd$_3$N@C$_{80}$(OH)$_{26}$(CH$_2$CH$_2$COOM)$_{16}$ (carboxyl)-**II**[5]	154 ± 7 (0.35 T)	207 ± 9 (2.4 T)	76 ± 3 (9.4 T)	78
Gd$_3$N@C$_{80}$O$_{11}$(OH)$_{21}$[9]	137 (0.47 T)	140 (1.4 T)[b]	58 (9.4 T)	125
Magnevist or Omniscan	4−6	4−6	4−6	

[a]300 K. [b]310 K.

summarized in the Supporting Information (Table S3). The nuclear magnetic resonance relaxivity (r_i) of both compounds were evaluated by the general equation:

$$R_i = \frac{1}{T_i, \text{obs}} = \frac{1}{T_i, \text{H}_2\text{O}} + \frac{1}{T_i, \text{para}} = \frac{1}{T_i, \text{H}_2\text{O}} + r_i[\text{M}]$$

where T_1 and T_2 are longitudinal and transverse relaxation time, respectively. The relaxation rate (reciprocal of relaxation time) is determined by both diamagnetic (pure water) and paramagnetic (contrast agent) species, and the ratio of paramagnetic relaxation rate to the concentration is the relaxivity of the paramagnetic compound, which can be experimentally obtained by the slope of ($1/T_i$) versus concentration of the paramagnetic contrast agents.[35] These results can be compared with the relaxivity of the commercial contrast agents Magnevist and Omniscan, which exhibit much lower relaxivity at all magnetic field strengths (4−6 mM^{-1} s^{-1}) (Table 1).[36] The hydrodynamic size distribution is a contributing factor for the relaxivities of the nanoparticle derivatives. The aggregation of MRI contrast agents leads to bigger and slower tumbling complexes and increased rotational correlation times (τ_c); this subsequently results in enhanced relaxivities relative to smaller aggregation or nonaggregated agents. The number of hydroxyl groups is also a key factor for the relaxivity, facilitating the gadofullerenes to trap water molecules in their aggregates. The relaxivity values for the (amino)-**I** are significantly higher at all magnetic field strengths than the commercial agents, but are lower than (carboxyl)-**II**, especially at the clinical magnetic field strength. This could be due in part to the slightly larger aggregate size of the (carboxyl)-**II** nanoparticle; there is also a much larger number of hydroxyl groups (10 vs 26) directly attached to the fullerene cage surface, which could more efficiently undergo (OH−H$_2$O) hydrogen exchange reactions for the (carboxyl)-**II** nanoparticle. The nanoparticle Gd$_3$N@C$_{80}$O$_{11}$(OH)$_{21}$, recently reported by Zhang and co-workers, also exhibits high relaxivity at all magnetic field strengths and contains a large number of hydroxyl groups (21) on the fullerene cage surface.[9] As indicated in Table 1, the amino functionalized nanoparticle reported by Zheng and co-workers (Gd@C$_{82}$O$_{14}$(OH)$_{14}$(NH$_2$)$_6$) ostensibly exhibits much lower relaxivity at all magnetic field strengths. This is misleading because the data in Table 1 is on a molar basis and not gadolinium atoms per molecule (1 vs 3).[26]

Although the (carboxyl)-**II** exhibits somewhat higher relaxivity than the unconjugated (amino)-**I** as illustrated in Table 1, it is important to demonstrate that both nanoparticles exhibit similar relaxivities once they are conjugated to the IL-13 peptide. In Figure 7A, the inversion−recovery images obtained using a clinical MR scanner (3 T, 123 MHz) of 5 mm tubes containing various concentrations of the (amino)-**I** and commercial MR contrast agent, Magnevist. The 1.67 μM
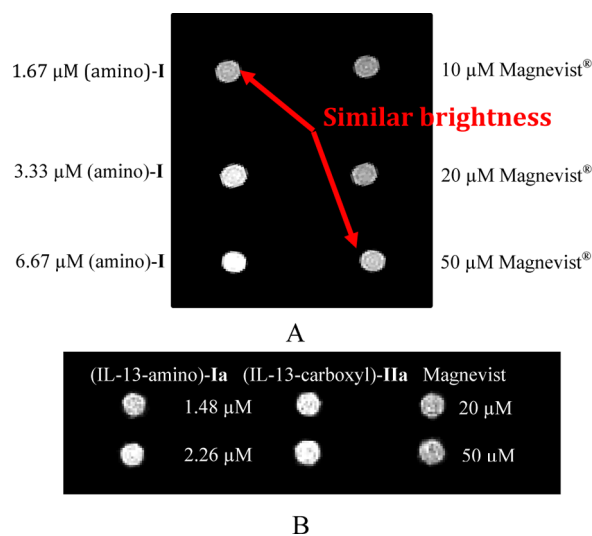

A

B

Figure 7. (A) Inversion−recovery MR images (T_1 = 1000 ms, T_R = 5000 ms, T_E = 30 ms) with (amino)-**I** and Magnevist as contrast agent. Left column from top to bottom: 1.67, 3.33, and 6.67 μM (amino)-**I** in water. Right column from top to bottom: 10, 20, and 50 μM commercial agent Magnevist in water. The 1.67 μM (amino)-**I** and 50 μM Magnevist in water exhibit comparable contrast. (B) Inversion−recovery MR images (T_1 = 1000 ms, T_R = 5000 ms, T_E = 30 ms) with (IL-13-amino)-**Ia** and (IL-13-carboxyl)-**IIa** and Magnevist as contrast agent. The conjugated nanoparticles exhibit similar contrast with the commercial contrast agent.

(amino)-**I** and 50 μM Magnevist in water share similar contrast. (IL-13-amino)-**Ia** at different concentrations (1.48 and 2.26 μM) is compared with the (IL-13-carboxyl)-**IIa** (1.48 μM and 2.26 μM) in Figure 7B. Even though the ^{1}H MR relaxivity of (amino)-**I** is less than that of (carboxyl)-**IIa**, after being conjugated with IL-13, both of them appear to give similar contrast at equal concentrations in the clinical 3 T MR image. Moreover, both the (IL-13-amino)-**Ia** and (IL-13-carboxyl)-**IIa** nanoparticles exhibit similar contrast at concentrations 20−50 times lower than commercial Magnevist.

The confocal microscopy studies (vide supra) of GBM U-251 cell tissue from orthotopically implanted U-251 GBM cell lines of both the (IL-13-amino)-**Ia** and (IL-13-carboxyl)-**IIa** nanoparticles demonstrate effective delivery of a targeting nanoparticle by noninvasive intravenous delivery. A 3 T MRI Siemens scanner was employed to demonstrate the potential clinical MRI feasibility of (IL-13-amino)-**Ia** and (IL-13-carboxyl)-**IIa** nanoparticles. In previous studies, we have shown that the (IL-13-carboxyl)-**IIa** nanoparticle provides excellent MRI contrast in animal GBM studies when administered by the invasive intracranial delivery approach CED.[25] In the current study, we find that both the (IL-13-amino)-**Ia** and (IL-13-carboxyl)-**IIa** provide targeting of
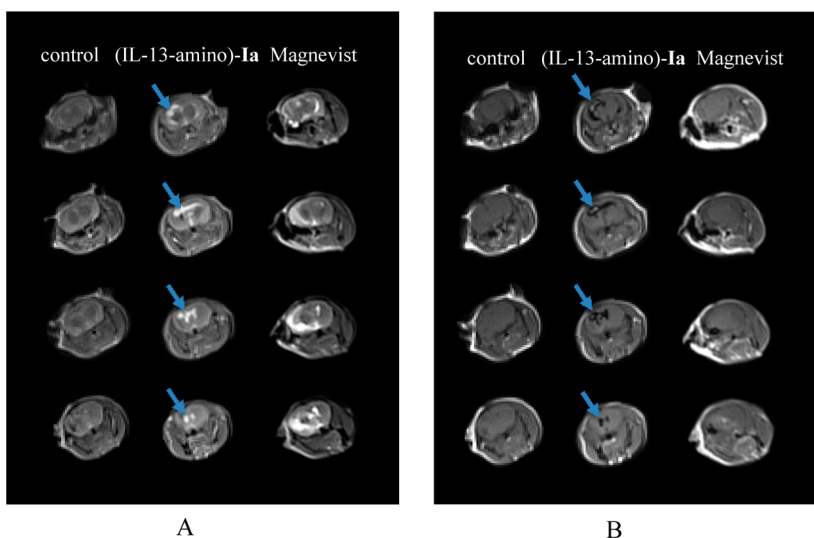
Figure 8. In vivo imaging following intravenous delivery of (IL-13-amino)-**Ia**. Left: MRI of a mouse brain without tumor as control. Middle: MRI of 15 min after intravenous injection of 300 μL ($\sim$0.9 nmol) of (IL-13-amino)-**Ia**. The bright contrast is due to the presence of (IL-13-amino)-**Ia**. Right: MRI of 15 min after intravenous injection of 100 μL (50 nmol) of Magnevist commercial contrast agent. Arrows indicate the location of tumor. (A) $T_1 = 50$ ms, $T_R = 5000$ ms, $T_E = 32$ ms. (B) $T_1 = 1000$ ms, $T_R = 5000$ ms, $T_E = 32$ ms.

orthotopically implanted U-251 tumor model via intravenous tail delivery. The MRI results for the (IL-13-carboxyl)-**IIa** nanoparticle clearly exhibit targeting to the mouse brain tumor model as illustrated in Figure S6. In an MR study with different inversion recovery times (50, 100, and 1000 ms), we have obtained 3 T MRI coronal images for the intravenously delivered (IL-13-amino)-**Ia** nanoparticle for a mouse model with U-251 tumor cells orthotopically implanted. In Figure 8 (middle) are illustrated the coronal slices for the shortest and longest inversion recovery times 50 and 1000 ms, respectively (100 ms MR data in Figure S7). These inversion recovery times illustrate a characteristic unique to the MR contrast characteristics of the f-Gd$_3$N@C$_{80}$ nanoparticle platform that is different from most other contrast agents. Specifically, Figure 8 shows that it is possible to track the material contrast with both T_1-weighted imaging characteristics where it shows high signal intensity with 50 ms inversion recovery times (bright tumor area). Whereas, T_2-weighted imaging is illustrated for 1000 ms inversion recovery times where low signal intensity is observed (dark tumor area). This is because the relaxivity ratio (r_1:r_2) is in a range that allows for T_1 enhancement while not overshortening T_2 and quenching the signal at low inversion recovery times, but quenching the signal at high inversion recovery times.[21] As a control, an animal without an implanted tumor is also shown (left, Figure 8). The (IL-13-amino)-**Ia** nanoparticle shows sharp definition of the tumor region in contrast with the indistinct tumor delineation of the control Magnevist (right, Figure 8) even at 1−2 orders of magnitude lower concentration. These results provide evidence that the nanoparticles (IL-13-amino)-**Ia** can be delivered by a less invasive intravenous injection approach with specific targeting of GBM U-251 mice brain tumor models and can be visualized at relatively low concentrations in a clinical MRI scanner.

4. CONCLUSIONS

In this paper, we report preparation of a new amino-surface functionalized Gd$_3$N@C$_{80}$ platform, characterized as Gd$_3$N@ C$_{80}$O$_{12}$(OH)$_{10}$(NH$_2$)$_7$(NO$_2$)$_2$ ((amino)-**I**), which was compared with a previously described hydrophilic, carboxyl-surface-

functionalized Gd$_3$N@C$_{80}$(OH)$_{26}$(CH$_2$CH$_2$COOM)$_{16}$ ((carboxyl)-**II**). We have found that this hydrophilic nanoparticle, when conjugated with an interleukin-13 peptide, IL-13-Gd$_3$N@ C$_{80}$O$_{12}$(OH)$_{10}$(NH$_2$)$_7$(NO$_2$)$_2$ ((IL-13-amino)-**Ia**), exhibits enhanced targeting of U-251 GBM cell lines. Our results support the notion that the (amino)-**I** positively charged nanoparticle exhibits enhanced charge attraction for GBM cellular endocytosis on the metallofullerene cage surface when directly compared with a carboxyl-surface functionalized nanoparticle, (IL-13-carboxyl)-**IIa**. Confocal microscopy results show that the (IL-13-amino)-**Ia** and (IL-13-carboxyl)-**IIa** both exhibit effective targeting of orthotopic GBM brain xenografts in mice by intravenous delivery. In similar fashion to the confocal microscopy results, we also demonstrate clinical MRI detection at low concentrations of this nanoparticle in U-251 GBM cells orthotopically implanted in mice. Although additional biodistribution and cytotoxicity studies are needed, the feasibility of these nanoparticles as potential new agents for diagnostic clinical MRI applications can be clearly forseen.

■ ASSOCIATED CONTENT

ⓢ Supporting Information

The structure of partial IL-13 sequence. The resulting atomic percentages of carbon and nitrogen. Confocal imaging of (IL-13-carboxyl)-**IIa** in HeLa, LN-18 and U-251. Confocal imaging of (ILs-13-amino)-**Is** and (ILs-13-carboxyl)-**IIs** in U-251. Fluorescent imaging of glioblastoma tumor after intracranial convection enhanced delivery and intravenous delivery of (IL-13-carboxyl)-**IIa**. In vivo imaging following intravenous delivery of (IL-13-amino)-**Ia** and (IL-13-carboxyl)-**IIa**. Comparison of relaxivities in pure water at 25 °C. The Supporting Information is available free of charge on the ACS Publications website at DOI: 10.1021/jacs.5b03991.

■ AUTHOR INFORMATION

Corresponding Authors
*hdorn@vt.edu
*zhisheng@vtc.vt.edu

Author Contributions

[⊥]T.L. and S.M. contributed equally.

Notes

■ ACKNOWLEDGMENTS

■ REFERENCES

(1) Kumar, H. R.; Zhong, X.; Sandoval, J. A.; Hickey, R. J.; Malkas, L. H. *Expert Rev. Neurother.* **2008**, *8*, 1497.

(2) Karathanasis, E.; Park, J.; Agarwal, A.; Patel, V.; Zhao, F.; Annapragada, A. V.; Hu, X.; Bellamkonda, R. V. *Nanotechnology* **2008**, *19*, 315101.

(3) Dubin, C. *Mech. Eng. Nanotechnol* **2004**, *126(S)*, 10.

(4) Kelkar, S. S.; Reineke, T. M. *Bioconjugate Chem.* **2011**, *22*, 1879.

(5) Shu, C. Y.; Corwin, F. D.; Zhang, J. F.; Chen, Z. J.; Reid, J. E.; Sun, M. H.; Xu, W.; Sim, J. H.; Wang, C. R.; Fatouros, P. P.; Esker, A. R.; Gibson, H. W.; Dorn, H. C. *Bioconjugate Chem.* **2009**, *20*, 1186.

(6) Fatouros, P. P.; Corwin, F. D.; Chen, Z. J.; Broaddus, W. C.; Tatum, J. L.; Kettenmann, B.; Ge, Z.; Gibson, H. W.; Russ, J. L.; Leonard, A. P.; Duchamp, J. C.; Dorn, H. C. *Radiology* **2006**, *240*, 756.

(7) Zhang, E. Y.; Shu, C. Y.; Feng, L.; Wang, C. R. *J. Phys. Chem. B* **2007**, *111*, 14223.

(8) Zhang, J. F.; Fatouros, P. P.; Shu, C. Y.; Reid, J.; Owens, L. S.; Cai, T.; Gibson, H. W.; Long, G. L.; Corwin, F. D.; Chen, Z. J.; Dorn, H. C. *Bioconjugate Chem.* **2010**, *21*, 610.

(9) Zhang, J. Y.; Ye, Y. Q.; Chen, Y.; Pregot, C.; Li, T. H.; Balasubramaniam, S.; Hobart, D. B.; Zhang, Y. F.; Wi, S.; Davis, R. M.; Madsen, L. A.; Morris, J. R.; LaConte, S. M.; Yee, G. T.; Dorn, H. C. *J. Am. Chem. Soc.* **2014**, *136*, 2630.

(10) MacFarland, D. K.; Walker, K. L.; Lenk, R. P.; Wilson, S. R.; Kumar, K.; Kepley, C. L.; Garbow, J. R. *J. Med. Chem.* **2008**, *51*, 3681.

(11) Verma, A.; Stellacci, F. *Small* **2010**, *6*, 12.

(12) Kardys, A. Y.; Bharali, D. J.; Mousa, S. A. *J. Nanotechnol.* **2013**, *2013*, 8.

(13) Zhu, H. R.; Gao, L.; Jiang, X. L.; Liu, R.; Wei, Y. T.; Wang, Y. L.; Zhao, Y. L.; Chai, Z. F.; Gao, X. Y. *Chem. Commun.* **2014**, *50*, 3695.

(14) Mikawa, M.; Kato, H.; Okumura, M.; Narazaki, M.; Kanazawa, Y.; Miwa, N.; Shinohara, H. *Bioconjugate Chem.* **2001**, *12*, 510.

(15) Kato, H.; Kanazawa, Y.; Okumura, M.; Taninaka, A.; Yokawa, T.; Shinohara, H. *J. Am. Chem. Soc.* **2003**, *125*, 4391.

(16) Bolskar, R. D.; Benedetto, A. F.; Husebo, L. O.; Price, R. E.; Jackson, E. F.; Wallace, S.; Wilson, L. J.; Alford, J. M. *J. Am. Chem. Soc.* **2003**, *125*, 5471.

(17) Sitharaman, B.; Bolskar, R. D.; Rusakova, I.; Wilson, L. J. *Nano Lett.* **2004**, *4*, 2373.

(18) Stevenson, S.; Rice, G.; Glass, T.; Harich, K.; Cromer, F.; Jordan, M. R.; Craft, J.; Hadju, E.; Bible, R.; Olmstead, M. M.; Maitra, K.; Fisher, A. J.; Balch, A. L.; Dorn, H. C. *Nature* **1999**, *402*, 898.

(19) Zhang, J. Y.; Stevenson, S.; Dorn, H. C. *Acc. Chem. Res.* **2013**, *46*, 1548.

(20) Fatouros, P. P.; Shultz, M. D. *Nanomedicine* **2013**, *8*, 1853.

(21) Shultz, M. D.; Wilson, J. D.; Fuller, C. E.; Zhang, J. Y.; Dorn, H. C.; Fatouros, P. P. *Radiology* **2011**, *261*, 136.

(22) Shultz, M. D.; Duchamp, J. C.; Wilson, J. D.; Shu, C. Y.; Ge, J. C.; Zhang, J. Y.; Gibson, H. W.; Fillmore, H. L.; Hirsch, J. I.; Dorn, H. C.; Fatouros, P. P. *J. Am. Chem. Soc.* **2010**, *132*, 4980.

(23) Debinski, W.; Gibo, D. M.; Slagle, B.; Powers, S. K.; Gillespie, G. Y. *Int. J. Oncol.* **1999**, *15*, 481.

(24) Debinski, W.; Gibo, D. M.; Hulet, S. W.; Connor, J. R.; Gillespie, G. Y. *Clin. Cancer Res.* **1999**, *5*, 985.

(25) Fillmore, H. L.; Shultz, M. D.; Henderson, S. C.; Cooper, P.; Broaddus, W. C.; Chen, Z. J.; Shu, C. Y.; Zhang, J.; Ge, J.; Dorn, H. C.; Corwin, F.; Hirsch, J. I.; Wilson, J.; Fatouros, P. P. *Nanomedicine* **2011**, *6*, 449.

(26) Zheng, J. P.; Zhen, M. M.; Ge, J. C.; Liu, Q. L.; Jiang, F.; Shu, C. Y.; Alhadlaq, H. A.; Wang, C. R. *Carbon* **2013**, *65*, 175.

(27) Lu, X.; Li, H.; Sun, B.; Shi, Z.; Gu, Z. *Carbon* **2005**, *43*, 1546.

(28) Sun, D. Y.; Huang, H. J.; Yang, S. H.; Liu, Z. Y.; Liu, S. Y. *Chem. Mater.* **1999**, *11*, 1003.

(29) Matsubayashi, K.; Kokubo, K.; Tategaki, H.; Kawahama, S.; Oshima, T. *Fuller. Nanotub. Car. N.* **2009**, *17*, 440.

(30) Yang, G.; Hu, H.; Zhou, Y.; Hu, Y.; Huang, H.; Nie, F.; Shi, W. *Sci. Rep.* **2012**, *2*, 698.

(31) Laus, S.; Sitharaman, B.; Toth, V.; Bolskar, R. D.; Helm, L.; Asokan, S.; Wong, M. S.; Wilson, L. J.; Merbach, A. E. *J. Am. Chem. Soc.* **2005**, *127*, 9368.

(32) Adiseshaiah, P.; Dellinger, A.; MacFarland, D.; Stern, S.; Dobrovolskaia, M.; Ileva, L.; Patri, A. K.; Bernardo, M.; Brooks, D. B.; Zhou, Z.; McNeil, S.; Kepley, C. *Invest. Radiol.* **2013**, *48*, 745.

(33) Brown, C. E.; Warden, C. D.; Starr, R.; Deng, X.; Badie, B.; Yuan, Y. C.; Forman, S. J.; Barish, M. E. *PLoS One* **2013**, *8*, e77769.

(34) Jacobs, V. L.; Valdes, P. A.; Hickey, W. F.; De Leo, J. A. *ASN Neuro* **2011**, *3*, 171.

(35) Caravan, P.; Ellison, J. J.; McMurry, T. J.; Lauffer, R. B. *Chem. Rev.* **1999**, *99*, 2293.

(36) Chang, C. A. *Invest. Radiol.* **1993**, *28*, S21.